Natural Resources Canada | Ressources naturelles Canada

CANMET Mining and Mineral Sciences Laboratories
Laboratoires des mines et des sciences minérales
DIVISION REPORT / RAPPORT DIVISION

Speciation and Characterization of Arsenic in Ketza River Mine Tailings Using X-ray Absorption Spectroscopy

D. Paktunc, A. Foster[1] and J.H.G. Laflamme
Mining and Mineral Sciences Laboratories
[1] U.S. Geological Survey Mineral Resources Division

May 2003

Published in Environmental Science & Technology, Volume 37, No. 10, 2003, pp. 2067-2074

Project: **MMSL No. 601212**
Advanced Mineral Characterization

DIVISION REPORT MMSL 03-036 (J)

104-05372/

Speciation and Characterization of Arsenic in Ketza River Mine Tailings Using X-ray Absorption Spectroscopy

DOGAN PAKTUNC,*,† ANDREA FOSTER,‡ AND GILLES LAFLAMME†

Canada Centre for Mineral and Energy Technology (CANMET), Mining and Mineral Sciences Laboratories, 555 Booth Street, Ottawa, Ontario K1A 0G1 Canada, and U.S. Geological Survey, Mineral Resources Division, 345 Middlefield Road, MS 901, Menlo Park, California 94025-3591

Ketza River mine tailings deposited underwater and those exposed near the tailings impoundment contain approximately 4 wt % As. Column-leaching tests indicated the potential for high As releases from the tailings. The tailings are composed dominantly of iron oxyhydroxides, quartz, calcite, dolomite, muscovite, ferric arsenates, and calcium−iron arsenates. Arsenopyrite and pyrite are trace constituents. Chemical compositions of iron oxyhydroxide and arsenate minerals are highly variable. The XANES spectra indicate that arsenic occurs as As(V) in tailings, but air-drying prior to analysis may have oxidized lower-valent As. The EXAFS spectra indicate As−Fe distances of 3.35−3.36 Å for the exposed tailings and 3.33−3.35 Å for the saturated tailings with coordination numbers of 0.96−1.11 and 0.46−0.64, respectively. The As−Ca interatomic distances ranging from 4.15 to 4.18 Å and the coordination numbers of 4.12−4.58 confirm the presence of calcium−iron arsenates in the tailings. These results suggest that ferric arsenates and inner-sphere corner sharing or bidentate−binuclear attachment of arsenate tetrahedra onto iron hydroxide octahedra are the dominant form of As in the tailings. EXAFS spectra indicate that the exposed tailings are richer in arsenate minerals whereas the saturated tailings are dominated by the iron oxyhydroxides, which could help explain the greater release of As from the exposed tailings during leaching tests. It is postulated that the dissolution of ferric arsenates during flow-through experiments caused the high As releases from both types of tailings. Arsenic tied to iron oxyhydroxides as adsorbed species are considered stable; however, iron oxyhydroxides having low Fe/As molar ratios may not be as stable. Continued As releases from the tailings are likely due to dissolution of both ferric and calcium−iron arsenates and desorption of As from high-As bearing iron oxyhydroxides during aging.

* Corresponding author e-mail: dpaktunc@NRCan.gc.ca; telephone: (613)947-7061; fax: (613)996-9673.
† CANMET.
‡ U.S. Geological Survey.

10.1021/es026185m CCC: $25.00 Published on Web 04/04/2003

Published 2003 by the Am. Chem. Soc.

Introduction

Arsenic is a common contaminant in tailings and effluents resulting from metallurgical processing of gold ores. In tailings, arsenic occurs in various forms such as arsenopyrite, arsenian pyrite, arsenates, and As-bearing iron oxyhydroxides. Stability of such arsenic minerals and compounds in metallurgical wastes for long-term disposal is one of the challenges facing the mining industry today. Recent epidemiological findings on the toxicological effects of As in drinking water in Bangladesh and India and worldwide revision of the drinking water standards for As have the potential to effect the current mining effluent guidelines. Tailings resulting from mining and milling operations constitute one of the important anthropogenic sources of arsenic in the environment. Effluent discharges containing arsenic have the potential to adversely affect the water quality of receiving waters.

The Ketza River mine is a former gold mine in south-central Yukon (Canada) operated for a brief period from 1988 to 1990. The gold mineralization was discovered in 1954. Two types of ore were delineated: 189 605 t of sulfide ore grading 11.3 g/t Au and 495 800 t of oxide ore grading 18 g/t Au. The mine produced over 2.8 t (100 000 oz.) of gold by mining and processing the oxide ore through a 320 t/day mill employing conventional carbon-in-pulp (CIP) cyanidation leach. Approximately 310 000 t of tailings was produced and deposited in the tailings impoundment under partial water cover. The tailings in the impoundment contain on average 4% As (*1*). Column-leaching studies on the tailings (*2*) indicated the potential for high arsenic releases from the tailings impoundment. Accordingly, several studies were conducted with the objective to determine the mineralogical composition of the tailings and the role of mineralogy in arsenic releases (*1*, *3*). Complexity of the arsenic mineralogy and the widespread occurrence of As-bearing iron oxyhydroxides as demonstrated by these studies necessitated that further detailed speciation and characterization studies be undertaken at the molecular scale to better determine the form, nature, and distribution of arsenic in the tailings. This is because arsenic mobilization from the tailings impoundment would be controlled by not only the dissolution processes but also the desorption−adsorption reactions involving iron oxyhydroxides.

Previous studies (*4*−*6*) utilizing synchrotron-based X-ray absorption spectroscopy have established that As(V) adsorbs on iron oxyhydroxide surfaces as inner-sphere complexes. O'Reilly et al. (*7*) studied the kinetics of arsenate sorption and desorption on goethite and found that the molecular environment did not change over extended periods. Foster et al. (*8*) and Savage et al. (*9*) demonstrated the usefulness of the X-ray absorption spectroscopy in the study of mine tailings comprised of mixed arsenic species. These studies made it clear that an understanding of the geochemical processes controlling As mobility cannot be achieved unless the mineralogical/chemical composition of the As sources at molecular scale are known. Accordingly, this study was carried out with the objective to determine the speciation and characteristics of arsenic along with their implications on the potential mobilization of arsenic from the tailings. The role of the milling process on the stability of the arsenic compounds in the tailings is discussed by Paktunc et al. (*3*). Along with the knowledge of geochemical processes controlling arsenic mobility, the source characteristics will help to develop better prediction of arsenic releases from the tailings

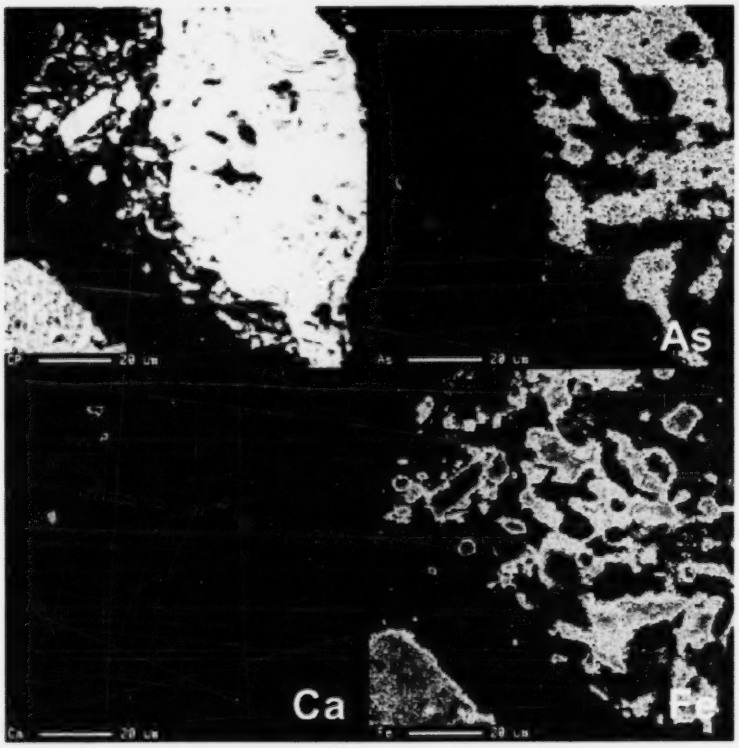

FIGURE 1. Backscattered electron photomicrograph and wavelength-dispersive X-ray maps of As-bearing iron oxyhydroxide and ferric arsenate displaying colloform banding.

and to design control and treatment options for long-term containment of the tailings.

Methodology

Samples. Samples from the tailings impoundment, B1 and B7, represent the exposed tailings and water-saturated tailings, respectively. The exposed tailings are dry tailings exposed at the periphery of the pond (*2*). The water-saturated tailings are from the bottom of the pond. Both tailings have particles that are less than 350 μm and possess similar particle size distributions. These tailings were subjected to column-leaching tests under water cover and steady-state conditions and with no cover and weekly flow-through flushing by the Pollution Abatement Division of Environment Canada in Whitehorse, YK (*2*). The residual tailings after column-leaching tests of up to 1-yr duration were labeled as C1 (exposed tailings after water cover leaching), C2 (exposed tailings following flow-through leaching), C7 (saturated tailings after flow-through leaching), and C8 (saturated tailings after water cover leaching). Both the original and residual tailings after column-leaching tests were dried at room temperature and sampled for mineralogical and spectroscopic studies.

Mineralogy. The tailings were characterized by a combination of optical microscopy, scanning electron microscopy, electron microprobe, and X-ray powder diffraction techniques. The quantitative electron microprobe analyses were performed by wavelength dispersion spectrometry (WDS) on a JEOL 733 microanalyzer, operated at 20 kV with a beam current of 20 nA (cup reading). The following X-ray lines and standards were used: Fe Kα (synthetic Fe_2O_3), Mn Kα (synthetic $MnTiO_3$), Ca Kα (sphene), Al Kα (synthetic $MgAl_2O_4$), As Lα (synthetic InAs), Si Kα (wollastonite), and S Kα (synthetic $PbSO_4$). Counting time was of the order of 40 s for the minor and trace elements, and raw data corrections were applied for ZAF (i.e., correction for atomic number, absorption, and fluorescence effects in X-ray microanalysis). The samples were also examined using a Rigaku rotating anode X-ray powder diffractometer with Cu Kα radiation at 55kV, 180 mA, step-scan of 0.04°, and scan rate at 4°/min in 2θ. The bulk samples were analyzed for Si, Ti, Al, Fe^{3+}, Fe^{2+}, Mn, Mg, Ca, Na, K, S, As, S, and C.

X-ray Absorption Spectroscopy (XAFS). The XAFS experiments were carried out at the Stanford Synchrotron Radiation Laboratory on wiggler beamline 4-3 and bending magnet beamline 2-3. Samples were mixed with boron nitride to produce an absorption length (μx, where μ is the mass absorption coefficient of the sample and x is the sample thickness) of ≈1 and loaded into Teflon holders with Mylar windows. A silicon (220) double-crystal monochromator with 1-mm vertical slits was used. The monochromator was detuned to 50% to eliminate harmonics. Arsenic foil was placed between the second and third ionization chambers for energy calibration at the inflection point of 11867.0 eV. N_2 gas was used in the first and second ionization chambers, and Ar gas was used in the third. Xe or Ar gas was used in the fourth (fluorescence) detector. XAFS spectra were collected both in the fluorescence mode (samples oriented at 45° with respect to the incident beam) using a Lytle detector and transmission mode (samples perpendicular to the incident beam) at room temperature. XANES spectra were obtained by scanning the monochromator at 0.2-eV steps over the edge region and the EXAFS spectra at 1.8−6.2 eV steps over the EXAFS region. The elapsed time for collection of a single XANES scan was 10 min and for an EXAFS scan was 30−40 min. Typically, four EXAFS scans were collected

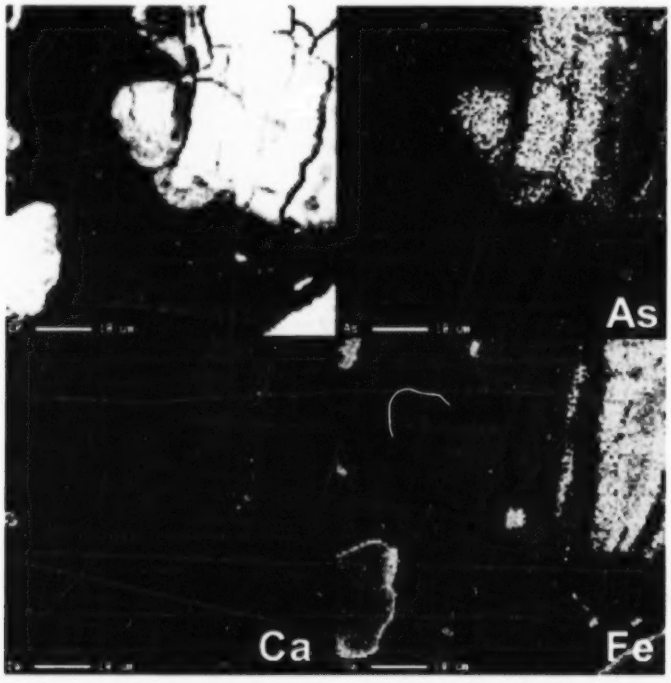

FIGURE 2. Backscattered electron photomicrograph and X-ray maps of ferric arsenate and calcium−iron arsenate in alternating bands.

for each sample and averaged to increase signal-to-noise ratio; therefore, the overall data collection time per sample was about 2.5 h. The EXAFSPAK software (*10*) was used for data reduction, which included the standard procedures of background subtraction, per atom normalization by a victoreen polynomial, and extraction of the EXAFS by a cubic spline function anchored on the low-energy side at 11,885 eV. In addition, IFFEFIT (*11*), Athena (*12*), and LSFitXAFS (*13*) were used for various data processing operations and least-squares analysis of the EXAFS spectra. The curve-fitting program OPT in EXAFSPAK was employed for EXAFS data analysis, using theoretical phase and amplitude functions generated in FEFF7 (*14*) from scorodite ($FeAsO_4 \cdot 2H_2O$) and rauenthalite ($Ca_3(AsO_4)_2 \cdot 10H_2O$). A fixed value of 0.85 was used for the global amplitude reduction factor (S_0^2).

Results and Discussion

Mineralogical Composition. The exposed tailings are primarily composed of iron oxyhydroxides, quartz, calcite, dolomite, muscovite, scorodite, and calcium−iron arsenates (*1*). Mineralogy of the saturated tailings is similar to that of the exposed tailings. Iron oxyhydroxides are the dominant species in the original and leached tailings. Arsenopyrite, pyrite, pyrrhotite, an Fe−Bi−As phase, native gold, a Cu−Au phase, and jarosite occur in trace to minor concentrations. Arsenopyrite abundances as determined by image analysis do not exceed 0.1 wt % in the tailings (*1*). Arsenopyrite also occurs as a minor phase in the ore samples obtained from the stockpiles, confirming that only the oxide ore was mined and processed. The tailings are characterized by high Fe_2O_3 concentrations, ranging from 44.0 to 68.2 wt %, and high As levels in the 3.7−4.4 wt % range. In terms of bulk composition, the exposed tailings have slightly higher Si, Ca, and Mg but lower Fe concentrations than the saturated tailings. There are no apparent mineralogical changes resulting from column-leaching experiments with the exception of flow-through leaching of the exposed tailings. In this case, calcite and dolomite appeared to have dissolved during the leaching experiments. This is also reflected by the bulk composition of the exposed tailings after flow-through leaching where differences of 5.1 and 0.4 wt % were noted in the measured Ca and Mg concentrations, respectively.

Iron oxyhydroxides occur essentially as discrete particles displaying zoning and colloform banding (Figure 1). In addition, iron oxyhydroxides occur as secondary reaction products on pyrite and arsenopyrite grains and as replacement products along the grain boundaries and microfractures in pyrite and arsenopyrite. Electron microprobe analyses indicate that iron oxyhydroxides have variable and elevated levels of As and Ca. In addition, some iron oxyhydroxide particles contain low levels of Al, Si, Mn, and S. Scorodite and other arsenates occur as discrete particles, as fine-grained agglomerations, and as replacement products after arsenopyrite. Arsenates may occur in association with As-bearing iron oxyhydroxide, displaying a colloform texture and enclosing anhedral fragments of pyrite. Intimate association of iron oxyhydroxides with variable levels of As and ferric arsenates in successive bands (Figure 2) is suggestive of precipitation and coprecipitation in close intervals. Calcium−iron arsenates including arseniosiderite ($Ca_2Fe_3(AsO_4)_3O_2 \cdot 3H_2O$) and yukonite ($Ca_2Fe_3(AsO_4)_4(OH) \cdot 12H_2O$) occur as massive, compositionally zoned particles; leaf-like aggregates with radial growth textures; spheroidal aggregates; and replacement products of arsenopyrite and scorodite. Jarosite is a trace phase, which occurs as a heterogeneous phase with variable arsenic concentrations. Arsenopyrite occurs as relict particles embedded in scorodite, iron−calcium arsenate hydrate, and arsenic-bearing goethite particles.

Chemical compositions of iron oxyhydroxide and arsenate compounds are highly variable, as shown in Figures 3 and 4. Iron oxyhydroxides contain variable As concentrations from trace (i.e., 300 ppm) to very high levels (i.e., 27.5%). On the Fe_2O_3 versus As_2O_5 plot, iron oxyhydroxides cluster in an array pointing toward scorodite and calcium−iron arsenate

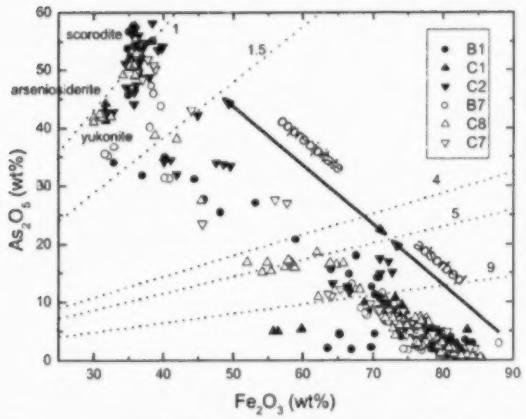

FIGURE 3. Variation of As_2O_5 as a function of Fe_2O_3 in iron oxyhydroxides and arsenates of the tailings. Dotted lines are Fe/As molar ratios. B1, exposed tailings; C1, exposed tailings leached under water cover; C2, exposed tailings leached under flow-through without water cover; B7, saturated tailings; C7, saturated tailings after flow-through leaching without water cover; C8, saturated tailings leached under water cover conditions.

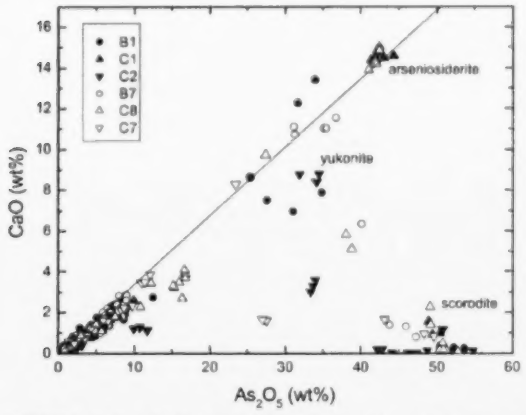

FIGURE 4. CaO vs As_2O_5 plot of iron oxyhydroxides and arsenates.

compositions from goethite and ferrihydrite compositions. Main clustering is confined to Fe/As molar ratios of 9 and greater. The other clustering on the Fe_2O_3 versus As_2O_5 plot is near scorodite and other arsenate compositions. Theoretical Fe/As molar ratios of the common arsenate minerals are between 1 and 1.5. Maximum As concentrations adsorbed onto iron oxyhydroxides during coprecipitation (*4*) correspond to an Fe/As molar ratio of about 1.5. Thus, grains having Fe/As molar ratios greater than 1.5 are considered to be iron oxyhydroxides in the data set.

The CaO levels in iron oxyhydroxides vary as a function of Fe_2O_3 and As_2O_5 concentrations. Like As_2O_5, CaO variation correlates negatively with Fe_2O_3. On the CaO versus As_2O_5 plot, iron oxyhydroxides cluster in an array pointing toward arseniosiderite and yukonite compositions (Figure 4).

XANES and EXAFS Analysis. XANES spectra indicate that arsenic occurs as As(V) in both exposed and saturated tailings (Figure 5). Because the saturated tailings were dried following the column-leaching studies, the XANES spectra may not be representative of the original underwater conditions. There is no indication of the presence of reduced arsenic species in the XANES spectra. However, contributions from reduced species that make up less than 10% of the bulk spectra would be difficult to reconcile.

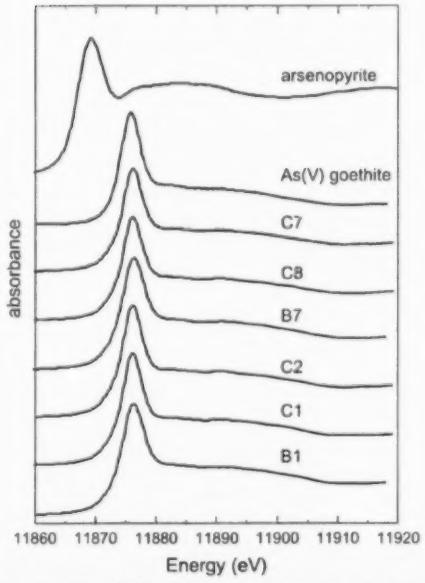

FIGURE 5. K-edge XANES spectra of arsenic in the tailings samples. Also shown are XANES spectra of As(V)-bearing goethite and arsenopyrite for comparison of the edge positions.

It is important to note that bulk XAFS represent a weighted sum of all contributions around As from a complex assemblage of As species that include stoichiometric As minerals and adsorbed/coprecipitated As. The weights are derived from the amount of arsenic contributed by each As-bearing species. In light of this, we have evaluated As speciation in these complex natural materials by two methods: the first is the pattern-matching approach utilizing model spectra of arsenic in several representative coordination environments from which we obtain quantitative estimates of the relative contribution of each As species to the total EXAFS spectrum. The second method is the classic shell-by-shell approach using phase and amplitude functions specific to each absorber−backscatterer pair (e.g., As−O and As−Fe) to obtain estimates for coordination numbers, distances, and static/thermal disorder (i.e., the Debye−Waller parameter). The results of pattern-matching fits are described first, followed by the results of shell-by-shell fits.

The k^3-weighted EXAFS spectra of the samples are shown in Figure 6. These spectra are sinusoidal waves representing constructive and destructive interference between the propagated and the reflected waves caused by the scattered electrons between the absorber and the neighboring atoms. The k^3-weighted EXAFS spectra of both saturated and exposed tailings resemble the model compound of As(V) adsorbed to goethite and amorphous ferric arsenate (Figure 6). Experimental EXAFS spectra obtained from model compounds and micro-XAFS spectra from discrete mineral particles in ore and cyanidation tailings from a bench-scale testwork (*15*) were used as end-members of the tailings' EXAFS spectra in the linear least-squares fits (*13*). Victoreen-normalized and k^3-weighted, smoothed EXAFS spectra were used in the fits. Variation in k was not allowed in the fit. The best fits were obtained with the addition of scorodite and three iron oxyhydroxides with different As concentrations (Table 1) as end-member components. The residual sum of squares values listed in Table 2 can be used as a measure of the goodness of the fit: the smaller the residual sum of squares, the better is the fit. The χ^2 values as the goodness-of-fit statistics vary from 0.37 to 0.62 and indicate that the fitting

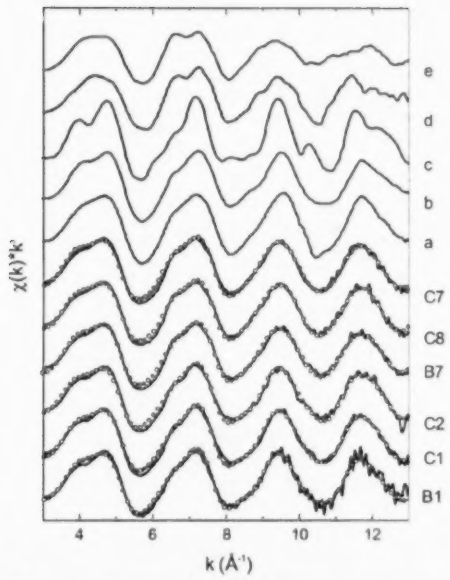

FIGURE 6. EXAFS spectra of the tailings samples and model compounds: (a) scorodite, (b) amorphous ferric arsenate, (c) arseniosiderite, (d) yukonite, and (e) As(V)-bearing goethite. Amorphous ferric arsenate and As-bearing goethite model compounds are as described by Foster et al. (*18*); Experimental curves are shown by solid lines, and the fitted spectra are shown by circles.

results are good within 95% probability. In addition, the total values provided in Table 2 can be used to assess the goodness-of-fit. Because the totals are not constrained in the fits, the closer the total to 100.0, the better is the fit. Foster et al. (*16*) estimated the errors in mineral quantities to be about 10% on least-squares fitting to XANES spectra. In the present case, uncertainties due to errors associated with the determination of $\chi(k)$ values were estimated from variations in the replicate EXAFS spectra from one sample. Fittings to EXAFS spectra of replicate scans resulted in the deviations of up to 19% from the mean values for mineral quantities greater than 10 wt % (Table 2). Uncertainties for individual components are given in Table 2.

Fourier transformation of the k^3-weighted EXAFS spectrum produces a radial structure function that can provide quantitative estimates of interatomic distances between the As atom and its nearest neighbors. Radial structure functions shown in Figure 7 are not corrected for phase shift, with the result that the interatomic distances are ≈0.5 Å less than true distances. The major peak in all the spectra, centered at approximately 1.3 Å, corresponds to scattering from O atoms (Figure 7). This is based on Fourier transformation of the model compounds listed in Table 1 of which the major peaks centered at approximately 1.3 Å correspond to scattering from O atoms in tetrahedral coordination. The second most prominent peak occurring at approximately 2.87 Å corresponds primarily to scattering from Fe atoms, based on analysis of scorodite, amorphous ferric arsenate, and As(V)-sorbed goethite model compounds (Table 1). The third prominent peak occurs at approximately 3.3 Å. In arseniosiderite and yukonite model compounds, this peak corresponds to scattering from Ca atoms, so in tailings samples this peak was also identified as arising from Ca atoms. These three major peaks were isolated and backtransformed to k space to form individual filtered EXAFS oscillations. Using phase and amplitude functions derived from model compounds, the filtered spectra were fit by nonlinear least-squares methods to estimate coordination numbers, distances, and

TABLE 1. Local Coordination Environment around a Central As Atom for the Model Compounds[a]

sample	shell	CN	R (Å)	σ^2 (Å^2)	E_0 (eV)
As(V)-goethite	As–O	4*	1.69	0.0006	−4.3
	As–Fe	0.45	2.85	0.004*	**
	As–Fe	1.29	3.29	0.004*	**
am. fer. arsenate	As–O	4*	1.70	0.0019	−2.2
	As–Fe	1.23	3.37	0.004*	**
	As–Fe	0.33	3.60	0.004*	**
scorodite	As–O	6.45	1.68	0.003	−6
	As–Fe	4*	3.36	0.004	**
arseniosiderite	As–O	4.25	1.71	0.0026*	−1.6
	As–Fe	3.66	3.29	0.0139	**
	As–Ca	2.44	4.24	0.0114	**
yukonite	As–O	4.00	1.71	0.0038*	−3.7
	As–Fe	3.24	3.28	0.0127	**
	As–Ca	4.17	4.21	0.0171	**
18CC (scorodite)	As–O	3.63	1.68	0.0015	−8.5
	As–Fe	2.50	3.36	0.0044	**
FeOxh2	As–O	4.15	1.69	0.0005	−10
	As–Fe	0.40	3.23	0.004*	**
	As–Ca	4.25	4.14	0.017*	**
	As-MS	21.75	3.13	0*	**
FeOxh8	As–O	4.76	1.69	0.0024	8.9
	As–Fe	0.12	3.33	0.004*	**
	As–Ca	4.52	4.14	0.017*	**
	As-MS	24.10	3.12	0*	**
FeOxh26	As–O	4.93	1.69	0.0029	−8
	As–Fe	0.19	3.27	0.004*	**
	As–Ca	3.56	4.17	0.017*	**
	As-MS	22.20	3.10	0*	

[a] Am. fer. arsenate, amorphous ferric arsenate; CN, coordination number; R, interatomic distance; σ^2, Debye–Waller parameter; E_0, energy offset; MS, multiple scattering. *, fixed value. **, value was fixed to the 1st shell E_0 value. FeOxh2, iron oxyhydroxide containing ~2% As_2O_5. FeOxh8, iron oxyhydroxide containing ~8% As_2O_5. FeOxh26, iron oxyhydroxide containing ~26% As_2O_5. 18CC (scorodite) and FeOxh2, -8, and -26 are based on micro-XAFS at PNC-CAT.

TABLE 2. Relative Abundances (wt %) of As Carriers Estimated by Least-Squares Fitting of Smoothed EXAFS Spectra to Individual Phases Analyzed by Micro-XAFS and a Model Compound[a]

	B1	C1	C2	B7	C8	C7
scorodite	31.4	31.1	31.3	13.1	5.5	13.5
am. fer. arsenate	44.2	40.3	34.2	43.6	37.5	36.1
FeOxh2	6.7	6.7	12.6	8.0	18.1	10.8
FeOxh8	17.7	21.8	21.9	35.4	36.6	33.9
FeOxh26					2.2	5.6
sum	100.0	99.9	100.0	100.1	99.9	99.9
rss	182	122	189	192	116	116
χ^2	0.58	0.39	0.60	0.61	0.37	0.37

[a] Fitting range (k), 3–13 Å^{-1}; rss, residual sum of squares. Scorodite is from a cyanidation tailings sample (18CC) analyzed by micro-XAFS. Am. fer. arsenate, amorphous ferric arsenate. FeOxh2, iron oxyhydroxide containing ~2% As_2O_5. FeOxh8, iron oxyhydroxide containing ~8% As_2O_5. FeOxh26, iron oxyhydroxide containing ~26% As_2O_5. Total number of experimental points ($\chi(k)k^3$) used in the fitting vary from 312 to 318. Estimated absolute deviations from the results: ±0.7 for scorodite, ±0.1 for am. fer. arsenate, ±3.2 for FeOxh2, ±0.7 for FeOxh8, and ±2.7 for FeOxh26.

Debye–Waller parameters. Because the fits employing three atomic shells (O, Fe, and Ca) resulted in displacements of the second and third neighbor peaks to longer interatomic distances (i.e., up to about 0.05 Å), a shell arising from multiple scattering (MS) of photoelectrons within the arsenate tetrahedron was added. This resulted in marked improvements to the fits as indicated by the goodness-of-fit parameters (Table 3). Addition of a MS shell to EXAFS fits is justified because of the similarity of the features to those attributed to MS by Foster et al. (*8*) and following Pandya (*17*) to

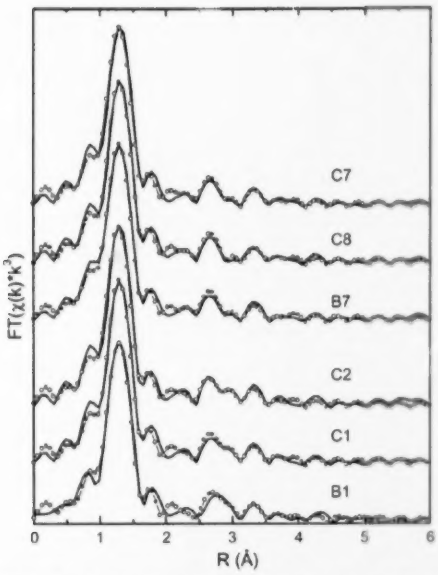

FIGURE 7. Fourier transformed spectra within *k* interval of 3−13 Å^{-1}. Radial distance not corrected for phase shift. Experimental curves are indicated by solid lines, and the lines with circles are those of the fitted spectra.

TABLE 3. EXAFS Fitting Results Summarizing the Local Coordination Environment around a Central Arsenic Atom[a]

sample	shell	CN	*R* (Å)	σ^2 (Å^2)	E_0 (eV)	ϵ^2
B1	As−O	5.02	1.69	0.0023	−5.3	
	As−Fe	1.11	3.35	0.004*	**	1.53
	As−Ca	4.12	4.17	0.0171*	**	1.54
	As-MS	18.20	3.14	0*	**	1.39
C1	As−O	4.90	1.69	0.0020	−4.9	
	As−Fe	0.96	3.36	0.004*	**	1.00
	As−Ca	4.38	4.18	0.0171*	**	0.95
	As-MS	21.71	3.14	0*	**	0.63
C2	As−O	4.85	1.69	0.0019	−7	
	As−Fe	0.99	3.36	0.004*	**	1.24
	As−Ca	4.30	4.15	0.0171*	**	1.21
	As-MS	22.36	3.12	0*	**	0.90
B7	As−O	5.09	1.69	0.0025	−5	
	As−Fe	0.54	3.35	0.004*	**	1.00
	As−Ca	4.21	4.18	0.0171*	**	0.96
	As-MS	23.90	3.12	0*	**	0.55
C8	As−O	4.77	1.69	0.0018	−5	
	As−Fe	0.46	3.33	0.004*	**	0.95
	As−Ca	4.50	4.18	0.0171*	**	0.89
	As-MS	22.69	3.13	0*	**	0.55
C7	As−O	4.96	1.69	0.0021	−6	
	As−Fe	0.64	3.34	0.004*	**	1.04
	As−Ca	4.58	4.17	0.0171*	**	0.99
	As-MS	22.15	3.12	0*	**	0.66

[a] CN, coordination number; *R*, interatomic distance; σ^2, Debye−Waller parameter; E_0, energy offset; ϵ^2, relative goodness-of-fit corresponding to the addition of the shell to all those preceding in order of decreasing importance; MS, multiple scattering. *, fixed value. **, value was fixed to the 1st shell E_0 value. Uncertainties in CN values: ±1.68 for As−O, ±0.40 for As−Fe, ±1.50 for As−Ca, and ±4.01 for As-MS. Uncertainties in *R* values: ±0.01 Å for As−O, ±0.02 Å for As−Fe, ±0.03 Å for As−Ca, and ±0.02 Å for As−MS estimated by comparing the EXAFS analysis of a scorodite to its nominal crystal structure parameters and highest standard deviations in the fits at 95% confidence limit.

adequately represent the first EXAFS oscillation of chromate EXAFS spectra. The Debye−Waller parameter for the MS shell was fixed to 0 as per Foster (*18*). The As−MS distances range from 3.12 to 3.14 Å (Table 3), which are comparable to those found by Foster (*18*) for MS in the arsenate tetrahedra of scorodite. Even accounting for the large estimated error (±20%) in EXAFS-derived coordination numbers, the coordination numbers varying from 18.2 to 23.9 for MS shells (Table 3) are significantly higher than the maximum of 12 double-scattering paths allowed for a tetrahedral anion. The overly high coordination numbers suggest that there is more amplitude to the As−MS shell than is accounted for by the theoretical phase and amplitude functions used to model it. The same trend is seen in the As−O shell, in which coordination numbers are also consistently higher than expected, but in this case, the high values fall within the range of the ideal value (4.0) if the estimated error of the parameter is considered. There are many possible reasons for the high coordination numbers in the MS shell fits, and discussing each in detail is beyond the scope of this paper. Briefly, the possibilities include (i) choice of the specific MS path chosen to represent the other 11 MS paths (the number of degenerate paths varies with the As−O bond lengths in the tetrahedron), (ii) choice of 0.85 as the value for S_0^2, a universal "damping" parameter that accounts for many-body ("shake-up" and "shake-off") electron effects arising from the central As atom (*19*), and (iii) unaccounted-for minor contributions to the EXAFS spectrum that influence the amplitude of the peak attributed to MS. Because the third shell of Ca atoms resulted in unrealistically high coordination numbers for this shell, a fixed Debye−Waller parameter obtained from fitting a shell of Ca atoms to yukonite and arseniosiderite model compounds was used. Significance of each shell in successive fits (i.e., O + Fe; O + Fe + Ca; O + Fe + Ca + MS) is indicated by the estimated statistical parameters for goodness-of-fit (*20*).

The fits indicate an As−O distance of 1.69 Å with a coordination number ranging between 4.77 and 5.09 (Table 3). The As−O bond length corresponds to tetrahedral coordination of oxygen atoms around As(V). In addition, a uniform As−Fe distance of 3.35−3.36 Å for the exposed tailings and their leached counterparts (Table 3) was obtained. Corresponding coordination numbers range from 0.96 to 1.11. In comparison, fits to the saturated tailings spectra produced slightly shorter As−Fe distances between 3.33 and 3.35 Å. Coordination numbers for the saturated tailings range from 0.46 to 0.64.

These distances are similar or slightly shorter than the average As−Fe interatomic distance in scorodite (i.e., 3.36 ± 0.02 Å) and greater than that resulting from bidentate−binuclear attachment of an arsenate tetrahedron to the apexes of two adjacent iron oxyhydroxide octahedra (i.e., 3.24−3.26 Å). Other possible inner-sphere adsorption geometries as outlined by Waychunas et al. (*5*, *21*, *22*) and Manceau (*23*) result in characteristic As−Fe interatomic distances of ~2.84 Å (bidentate−mononuclear arrangement) and 3.60 Å (monodentate−mononuclear arrangement). Although no evidence for the presence of the longer As−Fe distance is apparent in the tailings samples, the shorter distance is a possibility based on Fourier transformation between *k* values of 3 and 15.2 (*15*). Inclusion of a shorter Fe shell at ~2.8 Å was possible in some of the samples, but the approach of Thompson et al. (*20*) indicated that the improvement in the fitting results was insignificant within the fitting range of 3−13 Å^{-1}. EXAFS analysis of the arseniosiderite and yukonite models provided As−Fe distances of 3.29 and 3.28 Å, respectively. Accordingly, the contributions of arseniosiderite and yukonite to the bulk As−Fe distances cannot be ruled out. The As−Fe distances estimated for the iron oxyhydroxide-rich exposed tailings suggest that As sorbs to this material predominantly in a corner-sharing binuclear geometry. Iron coordination about a central As atom is 4 for scorodite and 3 for arseniosiderite. In the case of iron oxyhydroxides, Fe coordination is equal to or less than 2.

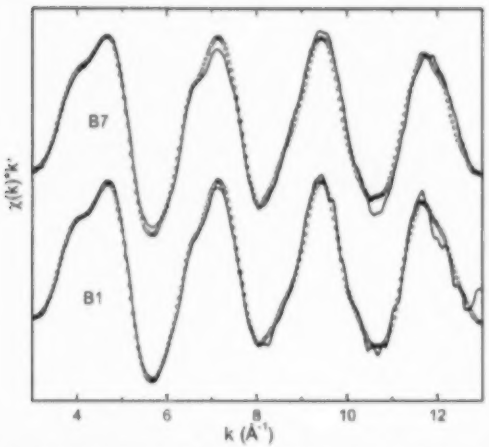

FIGURE 8. Least-squares fitting (circles) of the experimental EXAFS spectra (solid curves) to end-member phases listed in Table 1.

The As−Ca interatomic distances are relatively uniform ranging from 4.15 to 4.18 Å for the exposed tailings and from 4.17 to 4.18 Å for the saturated tailings. Corresponding coordination numbers range from 4.12 to 4.58. The As−Ca distances are slightly shorter but comparable to arseniosiderite (i.e., 4.24 Å) and yukonite (i.e., 4.21 Å). Coordination numbers are comparable as well and similar to the local coordination environments of yukonite and arseniosiderite (Table 1).

An independent assessment of the estimated mineral quantities by the pattern-matching approach was made with a mass balance consideration of the interatomic distances and coordination numbers (Figure 8). A mass balance treatment of the estimated mineral abundances listed in Table 2 and As−Fe interatomic distances of the end-member components indicate average radial distances of 3.35 Å for both saturated and exposed tailings. Both values are identical to the respective radial distances (i.e., 3.35 Å) determined by EXAFS analysis of the bulk samples. Similarly, the coordination numbers of the exposed tailings and saturated tailings calculated from the end-member components and their relative abundances based on least-squares fitting are 1.38 and 0.94, respectively. These are comparable to the coordination numbers determined by EXAFS analysis (i.e., 1.11 and 0.54).

Implications for Arsenic Mobilization. Arsenic releases of up to 17.9 and 34.7 mg/L from the exposed tailings leached under flow-through conditions (pH of 7−8) and between 1.1 and 3.9 mg/L under standing water cover conditions (pH of 6.5−7) were reported (*2*). Leaching results from the saturated tailings indicated lower As releases of up to 4.2 and 10.3 mg/L under flow-through (pH of 6−8) and between 0.3 and 2.6 mg/L under standing water cover conditions (pH of 6.5−7). Other than slightly higher carbonate concentrations in the exposed tailings, there are no apparent mineralogical differences between exposed and saturated tailings to account for the different leaching behavior. As indicated earlier, arsenopyrite and pyrite occur in trace to minor concentrations, and the particles are often surrounded by secondary arsenates or iron oxyhydroxides, thereby limiting their oxidative dissolution. Accordingly, contribution of sulfides to the observed arsenic releases from the exposed tailings would be insignificant. The mineral quantities listed in Table 2 are weight distribution of arsenic among the five phases that are assumed to represent the dominant arsenic carriers in the tailings. Scorodite forms approximately 31 wt % of the As-bearing minerals in the exposed tailings whereas it occurs less than about 13% in the saturated tailings. Amorphous ferric arsenate is abundant in all the tailings. The saturated tailings have greater abundances of the iron oxyhydroxides. In general, the results indicate that the exposed tailings are richer in arsenate minerals whereas the saturated tailings are dominated by the iron oxyhydroxides. This is based on the assumption that there were no significant changes in the speciation of As in the saturated tailings resulting from exposure to air oxidation during sample preparation. Experimental work of Randall et al. (*24*) and observations in buried sediments (*25*) indicate that As(V) species remain intact on iron oxyhydroxides rather than transforming to As(III) species under reducing conditions. Although transformation of aqueous As(V) species to As(III) can occur rapidly, this does not appear to be the case for As(V) sorbed to iron oxyhydroxides (*26*). Even if As(III) formed on iron oxyhydroxide surfaces, its rapid oxidation to As(V) during air-drying of the tailings would be unlikely based on the experimental results of Manning et al. (*27*) in that As(III) remains stable on goethite surfaces during air-drying. Furthermore, there are no indications for the establishment of sustained reducing conditions in the saturated tailings such as the presence of organic matter and secondary sulfide formation (*28*).

Higher abundances of the arsenate minerals and lower iron oxyhydroxide indicated by the EXAFS spectra of the exposed tailings could help explain higher As releases from the exposed tailings. It is plausible that the decreased quantities of amorphous ferric arsenate in the tailings leached by the flow-through experiments (i.e., C2 and C7) are indicative of the dissolution of amorphous ferric arsenate with resultant higher As releases.

The pH of the tailings pond water ranges from 7.4 to 8.8 with an average value of about 8.3. Under such conditions, ferric arsenates are in general regarded as thermodynamically unstable (e.g., ref *29*). This is especially the case for compounds with Fe/As ratios being less than 4 since the solubility of ferric arsenate compounds decreases with increasing Fe/As ratios (*30*). Calcium−iron arsenates have much higher solubilities than those of ferric arsenates (*31*). With the consideration that ferric arsenates and calcium−iron arsenates are less stable than iron oxyhydroxides in near surface environments, higher As releases from the exposed tailings with higher arsenate concentrations would not be surprising.

The nature of As on iron oxyhydroxide surfaces is another determining factor for As mobility from the tailings. On the basis of the preceding discussions, it appears that arsenate ions occur predominantly as bidentate complexes on iron oxyhydroxides. This is similar to the findings of Waychunas et al. (*5*, *21*, *22*) and Fendorf et al. (*6*) in that arsenate occurs predominantly as bidentate complexes and that monodentate arsenate complexes are present at lower As coverage. O'Reilly et al. (*7*) indicated that, following a rapid release of about one-third of arsenate from iron oxyhydroxide surfaces, desorption of arsenate bound to iron oxyhydroxides in a bidentate−binuclear manner would be limited with aging. Accordingly, arsenic tied to iron oxyhydroxides as adsorbed species would be considered as stable in near-surface environments.

The lowest Fe/As molar ratio of ferrihydrites is 5 for adsorption following ferrihydrite precipitation and 1.5 for adsorption during ferrihydrite precipitation based on saturation levels defined by Fuller et al. (*4*). According to Waychunas et al. (*5*), iron oxyhydroxides with arsenate near saturation limit (i.e., Fe/As = 1.5) consist of discrete dioctahedral Fe polymer chains with minimal cross-linking (i.e., smallest chains). This occurs due to coprecipitation of arsenate with ferrihydrite by retarding the growth of ferrihydrite. Cross-linking occurs in the absence of arsenate during ferrihydrite

precipitation. This form of coprecipitation is probably what some earlier researchers (e.g., ref *30*) referred to as "ferric arsenates" having Fe/As molar ratios of less than 4. Polymerization with aging of such iron oxyhydroxides with high arsenate probably results in the release of As. Accordingly, they are not considered as stable as the other iron oxyhydroxides with adsorbed As. Because the proportion of iron oxyhydroxides with Fe/As molar ratios of less than 5 is not insignificant (Figure 3), continued arsenic release from such iron oxyhydroxides by desorption during polymerization and aging of iron oxyhydroxides is likely to occur.

Acknowledgments

The project was funded in part by the Environmental Protection Branch of Environment Canada and the Natural Resources Canada's synchrotron research initiative. Portions of this research were carried out at the Stanford Synchrotron Radiation Laboratory, a national user facility operated by Stanford University on behalf of the U.S. Department of Energy, Office of Basic Energy Sciences. Micro-XAFS experiments were carried out at the Pacific Northwest Consortium-Collaborative Access Team's (PNC-CAT) beamline at the Advanced Photon Source (APS) in Argonne, funded by the Natural Sciences and Engineering Research Council of Canada through a major facilities access grant and by the U.S. Department of Energy under Contracts W-31-109-Eng-38 (APS) and DE-FG03-97ER45628 (PNC-CAT). Steve Heald's help with the experiments at PNC-CAT is greatly acknowledged. Eric Soprovich provided unpublished monitoring data from the Ketza River mine tailings impoundment. Arseniosiderite and yukonite mineral specimens were kindly provided by the British Museum through Peter Swash of Imperial College and the Canadian Museum of Nature. An interest in the copyright of this paper belongs to the Crown Her Majesty the Queen in right of Canada as represented by the Minister of Natural Resources.

Literature Cited

(1) Paktunc, A. D.; Szymanski, J.; Lastra, R.; Laflamme, G.; Enns, V.; Soprovich, E. In *Waste Characterization and Treatment*; Petruk, W., Ed.; Society for Mining, Metallurgy and Exploration, Inc.: 1998; pp 49–60.
(2) Soprovich, E. A. In *Seventh International Conference on Tailings and Mine Waste '00 Proceedings*, Fort Collins, CO; A. A.B-alkema: Rotterdam, 2000.
(3) Paktunc, A. D.; Laflamme, J. H. G.; Riveros, P. A.; Deschenes, G. *Arsenic mineralogy and bench-scale cyanidation testwork on composite materials from the Ketza River mine site, Yukon*; Mining and Mineral Sciences Laboratories Report MMSL 2000-017 (CR); CANMET: Ottawa, 2000.
(4) Fuller, C. C.; Davis, J. A.; Waychunas, G. A. *Geochim. Cosmochim. Acta* **1993**, *57*, 2271.
(5) Waychunas, G. A.; Rea, B. A.; Fuller, C. C.; Davis, J. A. *Geochim. Cosmochim. Acta* **1993**, *57*, 2251.
(6) Fendorf, S.; Eick, M. J.; Grossl, P.; Sparks, D. *Environ. Sci. Technol.* **1997**, *31*, 315.
(7) O'Reilly, S. E.; Strawn, D. G.; Sparks, D. L. *Soil Sci. Soc. Am. J.* **2001**, *65*, 67–77.
(8) Foster, A. L.; Brown, G. E.; Tingle, T. N.; Parks, G. A. *Am. Mineral.* **1998**, *83*, 553.
(9) Savage, K. S.; Tingle, T. N.; O'Day, P. A.; Waychunas, G. A.; Bird, D. K. *Appl. Geochem.* **2000**, *15*, 1219.
(10) George, G. N.; Pickering, I. J. *EXAFSPAK: a suite of computer programs for analysis of X-ray absorption spectra*; Stanford Synchrotron Radiation Laboratory: Stanford, CA, 1993.
(11) Newville, M. *J. Synchrotron Radiat.* **2001**, *8*, 322.
(12) Ravel, B. *ATHENA: an interactive graphical utility for processing EXAFS data* (unpublished computer program), 2002.
(13) Paktunc, D. *LSFitXAFS: A computer program for least squares fitting of bulk XAFS spectra to end-member components* (unpublished computer program), 2002.
(14) Zabinsky, S. I.; Rehr, J. J.; Ankudinov, A.; Albers, R. C.; Eller, M. J. *Phys. Rev.* **1995**, *B52*, 2995.
(15) Paktunc, D. CANMET, Mining and Mineral Sciences Laboratories, unpublished results.
(16) Foster, A. L.; Brown, G. E.; Parks, G. A. *Environ. Sci. Technol.* **1998**, *32*, 1444.
(17) Pandya, K. I. *Phys. Rev.* **1994**, *B50*, 15509–15515.
(18) Foster, A. L. Partitioning and Transformation of Arsenic and Selenium in Natural and Laboratory Systems. Ph.D. Thesis, Stanford University, 1999.
(19) Sayers, D. E.; Bunker, B. A. In *X-ray Absorption: Principles, Applications, and Techniques of EXAFS, SEXAFS and XANES*; Koningsberger, D. C., Prins, R., Eds.; John Wiley and Sons: New York, 1988; pp 211–253.
(20) Thompson, H. A.; Brown, G. E.; Parks, G. A. *Am. Mineral.* **1997**, *82*, 483.
(21) Waychunas, G. A.; Davis, J. A.; Fuller, C. C. *Geochim. Cosmochim. Acta* **1995**, *59*, 3655.
(22) Waychunas, G. A.; Fuller, C. C.; Rea, B. A.; Davis, J. A. *Geochim. Cosmochim. Acta* **1996**, *60*, 1765.
(23) Manceau, A. *Geochim. Cosmochim. Acta* **1995**, *59*, 3647.
(24) Randall, S. R.; Sherman, D. M.; Ragnarsdottir, K. V. *Geochim. Cosmochim. Acta* **2001**, *65*, 1015.
(25) Foster, A. L.; Breit, G. N.; Welch, A. H.; Whitney, J. W.; Yount, J. C.; Alam, M. M.; Islam, M. K.; Islam, M. N.; Islam, M. S. *EOS Trans. Am. Geophys. Union* **2000**, *81*, H21D-01.
(26) Langner, H. W.; Inskeep, W. P. *Environ. Sci. Technol.* **2000**, *34*, 3131.
(27) Manning, B. A.; Fendorf, S. E.; Goldberg, S. *Environ. Sci. Technol.* **1998**, *32*, 2383.
(28) Paktunc, D.; Dave, N. *Am. Mineral.* **2002**, *87*, 593.
(29) Robins, R. G. In *Arsenic metallurgy fundamentals and applications*; Reddy, R. G., Hendrix, J. L., Queneau, P. B., Eds.; TMS: Warrendale, PA, 1987; pp 215–247.
(30) Krause, E.; Ettel, V. A. *Hydrometallurgy* **1989**, *22*, 311.
(31) Swash, P. M.; Monhemius, A. J. In *Sudbury '95, Mining and the Environment Proceedings*; Hynes, T., Blanchette, M., Ed.; CANMET: Ottawa, 1995; pp 17–28.

Received for review September 24, 2002. Revised manuscript received February 21, 2003. Accepted March 6, 2003.

ES026185M